JCI insight

Effect of sex chromosomes versus hormones in neonatal lung injury

Sandra L. Grimm, … , Cristian Coarfa, Krithika Lingappan

JCI Insight. 2021. https://doi.org/10.1172/jci.insight.146863.

Research In-Press Preview Pulmonology

Graphical abstract

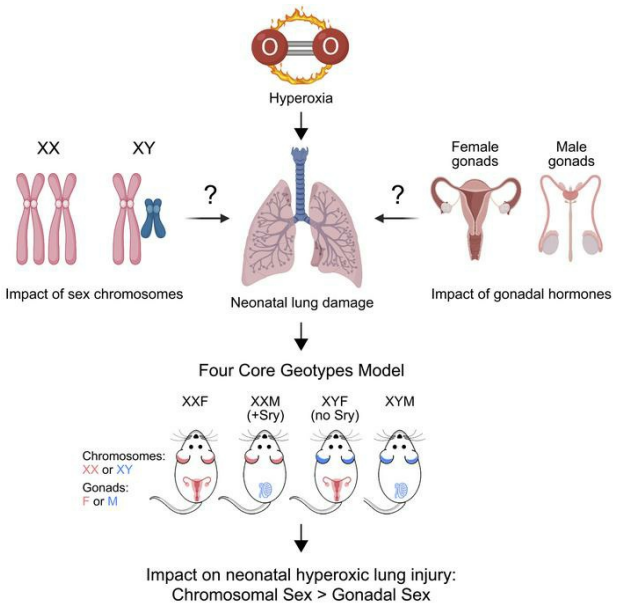

Effect of sex chromosomes versus hormones in neonatal lung injury

Sandra L. Grimm[1,2], Xiaoyu Dong[3], Yuhao Zhang[3], Alex Carisey[3], Arthur P. Arnold[4], Bhagavatula Moorthy[3], Cristian Coarfa[1,2,5], Krithika Lingappan[3]

Affiliation: [1]Molecular and Cellular Biology Department, Baylor College of Medicine, Houston, Texas, USA.

[2]Center for Precision Environmental Health, Baylor College of Medicine, Houston, Texas, USA.

[3]Department of Pediatrics, Texas Children's Hospital, Baylor College of Medicine, Houston, Texas, USA. Address: 1102 Bates Avenue, MC: FC530.01, Houston, Texas 77030.

[4] Integrative Biology and Physiology, University of California, Los Angeles

[5] Dan L Duncan Comprehensive Cancer Center, Baylor College of Medicine, Houston, Texas, USA.

Corresponding authors: Krithika Lingappan, Department of Pediatrics, Section of Neonatology, Texas Children's Hospital, Baylor College of Medicine, 1102 Bates Avenue, MC: FC530.01, Houston, Texas 77030. Phone: +1-832-824-3208. E-mail: lingappa@bcm.edu

Cristian Coarfa, Dan L Duncan Comprehensive Cancer Center, [4]Molecular and Cellular Biology Department, Baylor College of Medicine, Houston, Texas, USA. Phone: 713-798-7938. Email: coarfa@bcm.edu

The authors have declared that no conflict of interest exists.

Abstract:

The main mechanisms underlying sexually dimorphic outcomes in neonatal lung injury are unknown. We tested the hypothesis that hormonal- or sex chromosome-mediated mechanisms interact with hyperoxia exposure to impact injury and repair in the neonatal lung. To distinguish sex differences caused by gonadal hormones versus sex chromosome complement (XX versus XY), we used the four core genotypes (FCG) mice and exposed them to hyperoxia (95% FiO_2, PND1-4: saccular stage) or room air. This model generates XX and XY mice that each have either testes (with *Sry*, XXM or XYM) or ovaries (without *Sry*, XXF or XYF). Lung alveolarization and vascular development were more severely impacted in XYM and XYF compared to XXF and XXM mice. Cell cycle related pathways were enriched in the gonadal or chromosomal females, while muscle related pathways were enriched in the gonadal males, and immune-response related pathways were enriched in chromosomal males. Female gene signatures showed a negative correlation with human patients that developed BPD or needed oxygen therapy at 28 days. These results demonstrate that, chromosomal sex and not gonadal sex impacted the response to neonatal hyperoxia exposure. The female sex chromosomal complement was protective and could mediate sex-specific differences in the neonatal lung injury.

Introduction:

Sex as a biological variable plays a crucial role both during lung development and in modulating recovery from neonatal lung injury. Bronchopulmonary dysplasia (BPD), a lung disease characterized by aberrant alveolar and pulmonary vascular development, causes significant morbidity in preterm neonates. The incidence of this disease is skewed towards the male sex (1). In a recently published study from the Canadian Neonatal Network, among neonates born at <29 weeks' gestation between 2007 and 2016 the composite of death or major morbidity was higher in boys over the study period and the difference between rates of the major morbidities including BPD was unchanged between male and female premature neonates (2). The sex differences have been replicated in murine models and are strain specific (3, 4). Male mice have greater alveolar simplification, impaired pulmonary vascular development and more long-term adverse sequelae compared to female mice (5, 6).

The underlying molecular mechanisms behind these sex-specific differences may range from effects of sex chromosomes versus the differential exposure to sex hormones prenatally (7). To distinguish sex differences caused by gonadal hormones versus sex chromosome complement (XX versus XY), we used the four core genotypes mice (FCG) (8). In the FCG model (Figure 1) *Sry* is a transgene and is not present on the Y chromosome, so that XX and XY mice can each have either testes (with *Sry*, XXM or XYM) or ovaries (without *Sry*, XXF or XYF). The model also has an advantage in that it tests simultaneously for hormonal effects and the interaction of sex chromosome and hormonal effects. The XYM male (gonadal and chromosomal male) in this model bears the *Sry* gene on an autosome instead of the Y chromosome. When a wild-type

XXF female is bred with the XYM male, the pups could be any of the four genotypes: XXM (gonadal male with XX chromosomal complement), XYM (gonadal male with XY chromosomal complement), XXF (gonadal female with XX chromosomal complement), or XYF (gonadal female with XY chromosomal complement). Our objective was to test the hypothesis that hormonal or sex chromosome mechanisms interact in the sex-specific modulation of neonatal hyperoxic lung injury. We assessed changes in lung alveolarization and pulmonary vascular development after neonatal hyperoxia exposure (during the saccular stage of lung development PND1-4) in the FCG mice. In addition, differences in the pulmonary transcriptome and the underlying biological pathways and regulatory networks were elucidated and compared with changes in human patient gene expression stratified by sex (Figure 1).

Results:

Chromosomal Sex had a significant impact on alveolarization after neonatal hyperoxia exposure and not gonadal sex

Representative lung sections (PND21) stained with hematoxylin and eosin from the FCG mice (room air and hyperoxia-exposed) are shown in Figure 2A-D. Impact on lung alveolarization was measured using lung morphometric indices. The Mean Linear Intercept (MLI) and Radial Alveolar Count (RAC) were not different between the four genotypes at baseline under room air conditions (Figure 2E-F). Statistical analysis by 3-way ANOVA showed a main effect of treatment and chromosomal sex but not gonadal sex. Among the interactions, the interaction between chromosomal sex and treatment was statistically significant for RAC. The interaction between all

three factors (gonadal sex, treatment and chromosomal sex) was also significant. Compared to room air controls, the MLI was significantly increased in XYM mice. The RAC was decreased in all four genotypes upon exposure to hyperoxia. Compared to XYM and XYF mice, the XXM and the XXF mice had better preservation of the RAC upon exposure to hyperoxia. The detailed report of 3-ANOVA analysis is shown in Supplemental Table 1.

Arrest in angiogenesis after hyperoxia exposure is significantly impacted by chromosomal sex, but not gonadal sex

Pulmonary vessel density was determined based on Von Willebrand Factor (vWF) immunostaining, which is an endothelial-specific marker. vWF-stained vessels with external diameter (<50 μm per high-power field) were quantitated. Representative lung sections from room air and hyperoxia exposed mice at PND21 are shown in Figure 3A-D. Statistical analysis by 3-way ANOVA showed a main effect of treatment and chromosomal sex but not gonadal sex. The interaction between chromosomal sex and treatment was statistically significant. Compared to room air controls the vessel count was significantly decreased in XYM and XYF mice. Interestingly, the hyperoxia-exposed XXM and XXF mice were protected and had a higher vessel count compared to either the XYM or the XYF mice. We also performed immunohistochemistry for macrophages and quantitation of the same at PND21 (Figure 3F-J). Interestingly, we found compared to room air controls macrophages were increased in the hyperoxia-exposed lungs in XXF, XYM and XYF mice. Furthermore, the increased in XYM mice was greater compared to XYF mice.

Statistical analysis by 3-way ANOVA showed a significant effect of treatment and gonadal sex. The interaction between all three factors (gonadal sex, treatment and chromosomal sex) was also significant. The detailed report of 3-ANOVA analysis is shown in Supplemental Table 1.

Differences in the lung transcriptome in the FCG model after neonatal hyperoxia exposure

The FCG mice lung transcriptomes were profiled using RNA-Seq. The total number of up- and down-regulated differentially expressed genes (DEGs) in individual comparisons are shown in Figure 4. The hyperoxia responses (hyperoxia (O2) vs. normoxia (RA)) in each genotype are shown in Figure 4A, while differences between the genotypes in normoxia and under hyperoxic conditions are shown in Figure 4B and 4C respectively. In Figure 4A, at PND5, there are more down-regulated than up-regulated genes in all the genotypes except XYF mice. Interestingly, at PND21 the XYM mice had almost an equal number of up- and downregulated genes, whereas the other genotypes continued to have a predominance of downregulated genes. Genes on the X and Y chromosome were also analyzed. There were no genes on the Y chromosome that were differentially expressed in response to hyperoxia in the neonatal lung at PND5 or at PND21. There were 12 upregulated X-genes in XXF and 20 upregulated X-genes in XXM at PND5. At PND21, eight X-genes were upregulated in XXF and one gene in XXM. One of the common X-chromosome genes that was upregulated in XXM and XXF was apelin (*Apln*). Apelin is highly expressed in the vascular endothelium and attenuates hyperoxic lung and heart injury in neonatal rats (9). Four Y

chromosome genes (*Eif2s3y, Kdm5d, Ddx3y, and Uty)* were expressed to a greater extent in XY-mice compared to XX mice both under room air and hyperoxia at both the time-points. There were many X-chromosome specific genes that were higher in XX-mice under normoxia at PND5 which could have biased the response to hyperoxia in these mice. These genes included *Kdm5c* (XXF>XYM) and *Kdm6a* (XXM>XYM), which are both histone lysine demethylases and can thus modulate the epigenome and have been implicated in sexually dimorphic diseases (10). *Kdm6a* is a direct sensor of oxygen and controls chromatin and cell fate (11). *Kdm5c* has recently been implicated in sex-specific differences in adiposity (12) and interestingly is expressed to a greater extent in female HUVECs compared to male(13). The complete list of DEGs in each genotype at different time points as well as the X- and Y- chromosome specific genes is shown in Supplemental Table 2. The comparison of gene expression between chromosomally male and chromosomally female mice stratified for X-chromosome associated and autosomal genes on the four core genotypes mice under normoxic and hyperoxic conditions at PND5 and 21 is shown in Supplemental Figure 1.

Clustering of the FCG murine transcriptome responses based on chromosomal and gonadal patterns

To compare signatures (differentially expressed genes; DEGs) in our pulmonary murine models, we used transcriptome profiles of 578 healthy human adult lung samples compiled by the GTEx consortium, one of the largest scale efforts to assess genotype/transcriptome relationships in phenotypically healthy individuals (14). We

computed summed z-scores for each human individual and each FCG signature and assessed inter-signature correlations, as described in the supplemental material. There is a clear separation between the PND5 and the PND21 hyperoxia signatures, as shown in Figure 5A. The acute response signatures at PND5 show very strong correlation across all genotypes. Scatterplots presenting summed z-scores at individual specimen level, irrespective of biological sex, for all pairs of PND5 hyperoxia responses are shown in Supplemental Figure 2A. At PND21, the hyperoxia responses in gonadal or chromosomal females XXF, XXM, and XYF cluster together, separately from the XYM genotype. This pattern persisted despite separation of the human cohort into male and female samples as shown in Supplemental Figure 2B and 2C. Correlation of genotype summed z-scores in room air at PND5 show that signatures of comparisons between gonadal males and chromosomal males are highly correlated (Figure 5B). At PND21, however, signatures of male chromosomes over female chromosomes are highly correlated, as are signatures of male gonadal sex over female gonadal sex with the same sex chromosomal complement (Figure 5C). Next, correlation between genotype transcriptomic footprint in hyperoxia at PND5 indicated that all three signatures of male gonads over female gonads are highly correlated (Figure 5D). Finally, at PND21 there was a striking distinction with signatures of gonadal and chromosomal males clustering together as opposed to gonadal and chromosomal females (Figure 5E). For another perspective of the gene expression changes, we employed pathway-based cluster analysis for transcriptomic footprints of hyperoxia exposure or of genotype differences in the FCG model. Gene Set Enrichment Analysis (GSEA) was utilized to determine enrichment of GO

Biological Process pathways. Each transcriptomic response was represented based only on the normalized enriched scores (NES) of significantly enriched pathways (FDR<0.25), then hierarchical clustering was used to determine relationships between transcriptome responses. Pathway-based clustering of hyperoxia response across all FCG genotypes show clear clustering between the two time points PND5 (end of saccular stage of lung development) and PND21 (alveolar stage of lung development) (Figure 6A). Interestingly, while there are small differences according to sex variables in footprints at PND5, there was a fairly striking interaction of sex chromosomes and gonads at PND21. Similarly, pathway-based clustering of inter-genotype differences in room air conditions also showed a clear separation of the time points pointing towards a temporality in gene expression in the developing lung, (Figure 6B). Enriched biological pathways in inter-genotypes comparisons in hyperoxia show a disruption of the temporal patterns observed in room air (Figure 6C).

Effect of chromosomal and gonadal sex on gene expression in the developing lung in response to hyperoxia exposure:

We wanted to elucidate the DEGs in response to hyperoxia exposure based on the chromosomal and gonadal sex (Figure 7). The genes in region A depict the common DEGs between XXF and XYF (gonadal females), in region B depict the common DEGs between XXM and XYM (gonadal males), in region C include XXF and XXM (chromosomal female) and in region D include XYF and XYM (chromosomal male). These overlaps do not include the region E, which comprises of the common subset

of DEGs that were present in all the four genotypes (Figure 7A). Several interesting patterns emerge in this analysis. At PND5, the gonadal males and the chromosomal males have the greatest number of DEGs. In addition, with the exception of the female gonadal response which had 65.2% upregulated genes, all the other responses were comprised predominantly of downregulated genes. 76.5% of DEGs in the male gonadal response and 73.9% of DEGs in the female chromosomal response were downregulated. The male chromosomal response was more evenly distributed between up- and downregulated genes. At PND21, there was a predominant shift to mainly downregulated genes in all responses. In contrast, with the previous timepoint, the female gonadal and chromosomal response had the greatest number of DEGs. There were no upregulated genes in the male gonadal response. A detailed report of the number of DEGs in each genotype and the overlap based on gonadal or chromosomal sex is shown in Supplemental Figure 3. The overlap immediately after hyperoxia exposure was the highest between XYM and XYF mice with 40% of DEGs being common. The overlap was the least in the chromosomal female (XXM and XXF) mice at 18% and was about 30% in gonadal females and males. This overlap decreased in most genotypes at PND21, except in chromosomal females (XXM and XXF), where it increased to 24% from 18%. The overlap was least in gonadal males (between XYM and XXM) and was around 13% in gonadal females (XYF and XXF) and chromosomal males (XYM and XYF). In the common hyperoxia response in region E, there were 233 DEGs at PND5 (97 UP, 136 DOWN) and 27 DEGs at PND21. A detailed list of these genes is included in Supplemental Table 2.

Pathway analysis of DEGs: To identify biological processes that were enriched in gene signatures of FCG mice after exposure to hyperoxia, we used the Gene Ontology Biological Processes compendium. The number of enriched pathways and the overlap between gonadal and chromosomal sex is shown in Figure 8. At PND5, the highest overlap was seen between mice with male gonads (XXM,XYM) and male chromosomes (XYM and XYF) with 27.7% overlap. At PND21, however the greatest overlap was seen between female gonads and female chromosomes with 31.3% overlap. The other comparisons showed more common pathways at PND21 compared to PND5. The top 10 biological pathways enriched by gonadal or chromosomal sex are listed in Figure 9 along with their significance values and the number of included DEGs. At PND5, cell division and cytoskeletal organization pathways were enriched in mice with female gonadal sex (XXF and XYF), while in mice with female chromosomal sex (XXM and XXF) and male gonadal sex (XYM and XXM), almost all enriched pathways were related to muscle cell development or differentiation. Circulatory system development was one of the top pathways in XXM, XYM mice. In mice with male chromosomes (XYM and XYF), ion transport, cell motility and biological adhesion were among the top enriched pathways.

At PND 21, mice with female gonadal sex (XYF and XXF) and female chromosomal sex (XXF and XXM) were both enriched in pathways related to cell cycle and cell division. Pathways related to muscle contraction and muscle morphogenesis were enriched in mice with male gonadal sex. Interestingly, in mice with male chromosomal sex,

immune response related pathways predominated. Gene lists related to enriched pathways for all these comparisons are shown in Supplemental table 3.

We further focused on immune/inflammatory related and pathways related to lung development in this model (Supplemental Figure E3). As far as immune and inflammatory pathways are concerned, they were enriched in XXF mice at PND5 and in XXM mice at PND21 (Figure E3B). Interestingly, at PND21 the XXM mice have unique enrichment of these pathways compared to the other three genotypes. Many of these pathways are related to the innate immune response and inflammatory response to antigenic stimulus. Lung alveolus and epithelium development is enriched in XXF mice at PND5. At PND21, XYF mice show greater enrichment of lung development related pathways compared to the other three genotypes. Details of these pathways are provided in supplemental table 3.

Independent Real time qPCR validation: A subset of highly expressed differentially expressed genes were validated in an independent cohort of neonatal mice (Figure 10). The genes were selected based on the highest differential expression either based on gonadal sex or chromosomal sex at either time point. The fold change of the selected genes in the RNA-Seq experiment are shown in Figure 10A and the changes in the qRT-PCR experiments in Figure 10B (PND5) and 10C (PND21). The results and the known relevant biological significance are shown in Table 1. The detailed report of 3-ANOVA analysis is shown in Supplemental Table 1. Good correlation was seen for the validated genes between the RNA-Seq and the qRT-PCR results. For these

277 selected genes, we also evaluated the cell-specific expression using publicly available
278 neonatal lung single-cell expression database (LungMAP) in Figure 10D. At PND5, we
279 validated *Flt3* (FMS-like tyrosine kinase 3) *and Prokr2* (prokineticin receptor 2). *Flt3*
280 has the highest expression in myeloid cells and lymphocytes and *Prokr2* in
281 myofibroblasts in the murine lung at PND7. At PND21, we validated *Hamp* (hepcidin
282 antimicrobial peptide), *Peg 3* (Paternally expressed 3), *Zbtb16* (zinc finger and BTB
283 domain containing 16), and *Hif-3α* . At the cellular level, Hamp has the highest
284 expression in vascular endothelial cells, *Hif-3α* in the distal epithelium and the
285 lymphocytes, *Peg 3* in matrix fibroblasts, and *Zbtb16 in* endothelial cells and
286 lymphocytes at PND28 in the LungMAP dataset. In addition, we validated genes
287 related to inflammation/immune related pathways including *Tlr7* (Toll like receptor
288 7), *Nr1d1* (Nuclear Receptor Subfamily 1 Group D Member 1), *Alox15* (Arachidonate
289 15-Lipoxygenase), *Hk3* (Hexokinase 3), *Rsad2* (Radical S-Adenosyl Methionine
290 Domain Containing 2) and *Ltf* (Lactotransferrin) at PND21. The summary of the genes
291 and their known biological relevance is highlighted in the supplemental data (Table
292 1).
293

294 *Murine hyperoxia gene expression response associates with BPD blood transcriptomes*

295 A benefit of compiling transcriptomes in human clinical cohorts with rich clinical data
296 is enabling a statistical evaluation of the association between individual gene
297 signatures and clinical variables. We obtained blood transcriptome from a cohort of
298 human newborns (15) evaluated for development of BPD, and specifically analyzed

the human transcriptomes at PND28. We evaluated the distribution of summed z-scores for the hyperoxia gene signatures from all our murine models at PND21, over four clinical variables: gestational age, birth weight, BPD status and oxygen requirement at 28 days and also stratified the human samples by sex. Interestingly, we saw striking patterns between murine hyperoxia signatures at PND21 (Figure 11A-B). The XXF and XXM chromosomal female signatures were correlated with birth weight in the male blood samples (Supplemental Figure 4). However, the chromosomal or gonadal female (XXF, XXM, XYF) gene signatures were positively associated with birth weight, and anti-correlated with BPD and oxygen therapy at 28 days from the gene signatures from female patients. We next defined biological pathways that were upregulated in the human BPD patients at PND28, while suppressed after hyperoxia exposure in lungs of feminized mice and either induced or not differentially modulated in XYM mice at PND21 (Figure 11C). Interestingly pathways related to keratinization and muscle contraction were among the top significantly enriched pathways that showed this pattern of modulation.

Discussion:

In this study, we show for the first time the impact of chromosomal sex and gonadal sex on neonatal hyperoxic lung injury and repair in mice. Chromosomal sex and interaction between chromosomal sex and treatment had a significant effect on both alveolarization and pulmonary vascular development in hyperoxia exposed neonatal mice. Gonadal sex had a minor effect as evidenced by a significant three-way interaction between gonadal sex, chromosomal sex and hyperoxia for lung

development (Figure 2E and 2F). XXM and XXF were protected against hyperoxic lung injury compared to neonatal mice with XYM and XYF. We also report the changes in the lung transcriptome and the distinct enriched biological pathways that program the lung recovery after early life injury.

The sexual dimorphism in neonatal outcomes has been highlighted in many clinical and basic science publications. The developing fetus is exposed to gonadal hormones during organogenesis and many previous publications have reported on the deleterious effects of androgens on the developing lung (16). Conversely, the female sex hormones estrogens and progesterone are thought to have a protective effect (17, 18). However, after the immediate postnatal period, the developing lung is not exposed to high levels of circulating sex hormones; hence, hormone-independent effects could also underlie the sexual dimorphism seen in the neonatal lung. The four core genotypes (FCG) mouse model enables the separation of two main factors that underlie sex differences in disease pathophysiology: the sex chromosome complement (XX vs. XY) and the gonadal hormones. Using this model enabled us to compare XX and XY mice who were exposed to a comparable hormonal environment (19). Itoh *et al* showed that multiple copies of the *Sry* transgene are present in the FCG mice on chr 3 and that these mice do not show evidence of being exposed to different androgen levels prenatally (20). There were also no differences in postnatal gonadal hormonal levels between mice with a similar gonadal makeup (21).

344 The FCG model has been used to answer the question of whether it is the gonadal
345 hormones or the sex chromosomal complement to understand sexual dimorphism in
346 many diseases and processes including autoimmune diseases, stroke,
347 neurobehavioral derangements, nociception and drug abuse (19, 21). Interestingly,
348 in gonadectomized FCG mice, XY mice irrespective of gonadal sex, developed less
349 severe hypoxia-induced pulmonary hypertension than XX mice (22). In viral
350 infections, the sex chromosomal complement played a role in the pathogenesis and
351 outcomes associated with coxsackievirus B3 infections, but not with influenza A (23).
352 Indices of alveolarization and pulmonary vascular development were impaired to a
353 greater extent in hyperoxia-exposed XYM and XYF mice compared to similarly
354 exposed XXM and XXF mice. This led us to speculate that either Y-chromosome
355 specific genes were increasing susceptibility or genes that were expressed to a higher
356 extent in XXM and XXF mice due to incomplete X-inactivation (X-escapees) were
357 providing protection against hyperoxic lung injury. The increased overlap in
358 chromosomally female mice at PND21 when most other genotypes diverged, points
359 to a greater modulating effect of the female chromosomal sex on gene expression
360 after early hyperoxia exposure.
361
362 The biological pathways that were enriched by male or female gonadal or
363 chromosomal sex were distinct at PND5 and PND21. Since sex chromosomal effects
364 were significant in the lung phenotype at PND21, a closer examination of the enriched
365 biological pathways by chromosomal sex could identify new molecular targets for
366 pharmaco-chemical intervention. The enrichment of cell-cycle related pathways in

XX mice and immune related pathways in XY mice at PND21 may dictate the recovery response of these lungs following early hyperoxia exposure. The gene signatures in the hyperoxia exposed murine lungs in XXF, XXM, and XYF mice were anti-correlated with the BPD signature of human female preterm babies. This was not observed with the XYM mouse lung with either the male or the female human gene expression. This further leads us to speculate that the feminized lung modulates biological pathways that protect against hyperoxia-mediated lung injury which also correlate with decreased risk of BPD at least in human female infants.

There are limitations to this study. The use of 95% FiO2 during P1 to P4 (saccular stage of lung development) is high. The main reason to restrict the hyperoxia exposure to the first four postnatal days was to restrict the hyperoxia exposure during the saccular stage of lung development in mice(24). This corresponds to 26 to 36 weeks in human lung development (25). The diagnosis of BPD is made in human preterm neonates at 36 weeks of post menstrual age based on their level of respiratory support (26). For these reasons we chose to limit the hyperoxia exposure to the saccular stage of lung development for this manuscript. Prolonging the hyperoxia exposure to 14 days would correlate with human patients receiving hyperoxia throughout their first year of life and beyond. Our previous publications (27, 28) as well as publications from other labs (29–32) have shown the long-term effects of hyperoxia exposure during the saccular stage of lung development on the developing lung. However, the use of high FiO_2 may replicate the clinical course of babies with severe lung disease who need higher FiO_2 and are at greatest risk to

develop severe BPD. We used MLI and RAC as morphometric indices to describe the changes in the lung parenchyma. There are limitations to these indices for their use in quantitative morphology of the lung and have been expanded on excellent reviews (33, 34). The use of F4/80 immunostaining for quantitation of lung macrophages does not distinguish between resident alveolar and recruited macrophages and is expressed on other cells such as eosinophils (35). Whole lung RNA-Seq prevents the elucidation of cell-specific expression of DEGs. However, we attempted to speculate the cell-specific role of the selected DEGs based on the LungMAP database. Even though we showed that the chromosomal sex and not the gonadal sex had a profound effect on the injured neonatal lung during recovery, the protective effect of the double dose of the X chromosome versus the deleterious effect of the Y chromosome still needs to be clarified. Interestingly, in our study none of the Y chromosome genes were differentially modulated by hyperoxia exposure leading us to speculate that the attenuation of the lung injury in the XXF and XXM mice may be mediated through genes on the X chromosome. An X chromosome gene that escapes X-inactivation may be protective in the chromosomal female mice. Cell-specific expression of genes localized on the X chromosome will provide further insight. Species-related differences in X-inactivation also need to be taken into account. In humans, more X-chromosome linked genes escape inactivation compared to mice (36). The correlation between human blood samples and mouse lung samples is not ideal, but these findings may point to pathways that are altered systemically (including the lung) that play a role in disease pathogenesis and vary by biological sex.

In conclusion, using the FCG model to delineate the contribution of chromosomal sex versus gonadal sex in neonatal hyperoxic lung injury should be considered an important but preliminary step towards identifying the mechanisms behind sex specific differences in BPD. Depending on the sex chromosome complement the effect of gonadal hormones might vary. Our future directions will focus on identifying the specific genes on the X chromosome which could be mediating the protective effect in chromosomal females and to identify their expression patterns in the lung and mechanisms of action.

Methods:

Animals: FCG mice were obtained from Jackson Labs (Stock number: 010905) and bred according to the protocol. When a wild-type XXF female is bread with the XYM male (both on C57BL/6J background), the pups belong to any one of the four genotypes (XXM, XYM, XXF and XYF). Mice were genotyped by genomic PCR to detect the Y chromosome, *Sry*, and a control autosomal gene, as described (7).

Mouse Model of BPD: The FCG mouse pups were exposed to hyperoxia (95% O_2), as described previously to replicate the arrest of lung development as seen in human neonates with BPD (3, 37). Pups were euthanized on PND5 (immediately after hyperoxia exposure) or PND21 (after recovery in room air; during alveolar phase of lung development; **Figure 1**). Evaluation of lung morphometry (mean linear intercept and radial alveolar count), lung vascular development (immunohistochemistry for

436 vWF) and lung macrophage quantitation (immunohistochemistry for F4/80) was
437 performed at PND21 as previously described (3). The detailed protocol is included in
438 supplemental data.
439
440 **Analysis of the Whole Lung Transcriptome:** RNA-Seq analysis was performed on
441 the whole lung mRNA to analyze differences in the pulmonary transcriptome among
442 the FCG mice at the two time points: PND5 (end of saccular stage of lung
443 development) and PND21 (alveolar stage of lung development) as shown in Figure
444 1. Sex of the animals was ascertained using genotyping for the *Sry* (sex determining
445 region Y) gene. **Figure 1** also shows the RNA-Seq signal (defined as Fragments Per
446 Kilobase of transcript per Million mapped reads; FPKM) for *Uty* (a Y chromosome
447 specific gene), *Xist* (an X chromosome specific gene expressed only when more than
448 one X chromosome is present), and *Sry* in representative samples for each of the
449 experimental groups submitted for RNA-Seq analysis. The detailed methodology for
450 the RNA-Seq analysis is included in the supplemental data. The data set has been
451 deposited in NCBI GEO (GSE162853).
452
453 **Validation of RNA-Seq data:** qRT-PCR analysis was conducted on lung mRNA from
454 an independent cohort of FCG neonatal mice to validate the results of the RNA-Seq
455 analysis. The genes chosen and the primer information is included in the
456 supplemental data. The expression of these genes at the cellular level was predicted
457 using the LungMAP database (38, 39).
458

Human transcriptomic data mining:

Transcriptomes for healthy adult whole lung from the GTEx consortium were downloaded from the GTEx data portal. Blood transcriptome data from newborns was downloaded from NCBI GEO, accession number GSE32472 (15). The human transcriptome data mining and analysis is described in detail in the supplemental data.

Statistics: Data analysis for lung morphometry, pulmonary vascular development and gene expression validation was done using GraphPad Prism, version 9. Three-way ANOVA was used to assess the effect of gonadal sex, chromosomal sex and treatment as well as the interaction between the three independent variables. Comparison between individual groups was performed using Sidak's multiple comparisons test. The number of biological replicates is specified for each experiment. P value of <0.05 was considered statistically significant.

Study Approval: All studies were conducted at Baylor College of Medicine under the purview of the Institutional Animal Care and Use Committee (IACUC) (Protocol number AN-6474). Experiments were performed in accordance with the highest contemporary standards as per the IACUC protocols.

Author Contributions

Conception of projects and study design: KL; Conducting experiments, Data Analysis and Interpretation: KL, CC, SLG, APA; Drafting the manuscript and intellectual contribution: All Authors.

Acknowledgements

This project was supported by NIH grants R01 HL144775, R01 HL146395 and R21HD100862 to KL. SLG and CC were partially supported by the NCI P30 shared resource grant CA125123, CPRIT grant RP200504, P30 ES030285, and P50 MD015496. NIEHS center grant P30 ES030285. This study was partially supported by NIEHS grants 5R01ES029382, 5R01HL129794 and 1P42ES0327725 to BM. APA was supported by HD090637, HD100298, and HD076125.

References:

1. Peacock JL et al. Neonatal and infant outcome in boys and girls born very prematurely. *Pediatr Res.* 2012;71(3):305–310.

2. Garfinkle J et al. Trends in sex-specific differences in outcomes in extreme preterms: Progress or natural barriers?. *Arch Dis Child Fetal Neonatal Ed.* 2020; 105(2):158-163.

3. Lingappan K et al. Sex-specific differences in neonatal hyperoxic lung injury. *Am J Physiol Lung Cell Mol Physiol.* 2016;311(2): L481-493.

4. Leary S et al. Genetic Strain and Sex Differences in a Hyperoxia-Induced Mouse Model of Varying Severity of Bronchopulmonary Dysplasia. *Am J Pathol.* 2019; 189(5): 999-1014.

5. Namba F et al. Sex-related differences in long-term pulmonary outcomes of neonatal hyperoxia in mice. *Exp Lung Res.* 2016;42(2):57–65.

6. Gong J et al. Endothelial to mesenchymal transition during neonatal hyperoxia-induced pulmonary hypertension. *J Pathol.* 2020;252(4):411-422.

7. Arnold AP. A general theory of sexual differentiation. *J Neurosci Res.* 2017;95(1-2):291-300.

8. Burgoyne PS, Arnold AP. A primer on the use of mouse models for identifying direct sex chromosome effects that cause sex differences in non-gonadal tissues. [Internet]. *Biol Sex Differ.* 2016;7(1):68.

9. Visser YP et al. Apelin attenuates hyperoxic lung and heart injury in neonatal rats.

Am J Respir Crit Care Med. 2010;182(10):1239–1250.

10. Snell DM, Turner JMA. Sex Chromosome Effects on Male–Female Differences in Mammals. *Curr Biol.* 2018;28(22):R1313–R1324.

11. Chakraborty AA et al. Histone demethylase KDM6A directly senses oxygen to control chromatin and cell fate. *Science.* 2019;363(6432):1217-1222.

12. Link JC et al. X chromosome dosage of histone demethylase KDM5C determines sex differences in adiposity. *J Clin Invest.* 2020;130(11):5688–5702.

13. Hartman RJG et al. Intrinsic transcriptomic sex differences in human endothelial cells at birth and in adults are associated with coronary artery disease targets. *Sci Rep.* 2020;10(1):1–12.

14. Aguet F et al. Genetic effects on gene expression across human tissues. *Nature*. 2017;550(7675):204-213.

15. Pietrzyk JJ et al. Gene Expression Profiling in Preterm Infants: New Aspects of Bronchopulmonary Dysplasia Development. *PLoS One* 2013;8(10):e78585.

16. Nielsen HC. Androgen receptors influence the production of pulmonary surfactant in the testicular feminization mouse fetus. *J Clin Invest.* 1985;76(1):177–181.

17. Seaborn T et al. Sex hormone metabolism in lung development and maturation. *Trends Endocrinol Metab.* 2010;21(12):729–738.

18. Trotter A et al. Effects of postnatal estradiol and progesterone replacement in extremely preterm infants. *J Clin Endocrinol Metab.* 1999;84(12):4531–4535.

19. Arnold AP, Chen X. What does the “four core genotypes” mouse model tell us about sex differences in the brain and other tissues? *Front Neuroendocrinol.* 2009;30(1):1–9.

20. Itoh Y et al. Four core genotypes mouse model: localization of the Sry transgene and bioassay for testicular hormone levels. *BMC Res Notes* 2015;8(1):69.

21. Manwani B et al. Sex differences in ischemic stroke sensitivity are influenced by gonadal hormones, not by sex chromosome complement. *J Cereb Blood Flow Metab.* 2015;35(2):221–229.

22. Umar S et al. The Y Chromosome Plays a Protective Role in Experimental Hypoxic Pulmonary Hypertension. *Am J Respir Crit Care Med.* 2018;197(7):952–955.

23. Robinson DP et al. Sex chromosome complement contributes to sex differences in coxsackievirus B3 but not influenza A virus pathogenesis. *Biol Sex Differ.* 2011;2:8.

24. Benjamin JT et al. Neutrophilic inflammation during lung development disrupts elastin assembly and predisposes adult mice to COPD. *J Clin Invest.* 2021;131(1):e139481.

25. Whitsett JA et al. Building and regenerating the lung cell by cell. *Physiol Rev.* 2019;99(1):513-554.

26. Jobe AH, Bancalari E. Bronchopulmonary dysplasia. *Am J Respir Crit Care Med.*2001;163(7):1723–1729.

27. Coarfa C et al. Epigenetic response to hyperoxia in the neonatal lung is sexually

565 dimorphic. *Redox Biol.*2020;37:101718.

566 28. Zhang Y et al. Microrna-30a as a candidate underlying sex-specific differences in
567 neonatal hyperoxic lung injury: Implications for BPD. *Am J Physiol Lung Cell Mol*
568 *Physiol.* 2019;316(1). L144-156.

569 29. Yee M et al. Neonatal hyperoxia depletes pulmonary vein cardiomyocytes in
570 adult mice via mitochondrial oxidation. *Am J Physiol Lung Cell Mol Physiol.*
571 2019;(55):846–859.

572 30. Yee M, Buczynski BW, O'Reilly MA. Neonatal hyperoxia stimulates the expansion
573 of alveolar epithelial type II cells. *Am J Respir Cell Mol Biol*. 2014;50(4):757-766.

574 31. Cohen ED et al. Neonatal hyperoxia inhibits proliferation and survival of atrial
575 cardiomyocytes by suppressing fatty acid synthesis. *JCI Insight* 2021;6(5):e140785.

576 32. Buczynski BW et al. Neonatal hyperoxia alters the host response to influenza A
577 virus infection in adult mice through multiple pathways. *AJP Lung Cell Mol Physiol.*
578 2013;305(4):L282-90.

579 33. Hsia CCW et al. An Official Research Policy Statement of the American Thoracic
580 Society/European Respiratory Society: Standards for Quantitative Assessment of
581 Lung Structure. *Am J Respir Crit Care Med.* 2010;181(4):394–418.

582 34. Knudsen L et al. Assessment of air space size characteristics by intercept (chord)
583 measurement: an accurate and efficient stereological approach. *J Appl Physiol.*
584 2010;108(2):412–421.

585 35. Misharin AV et al. Flow cytometric analysis of macrophages and dendritic cell

586 subsets in the mouse lung. *Am J Respir Cell Mol Biol.*2013;49(4):503–510.

587 36. Berletch JB, Yang F, Disteche CM. Escape from X inactivation in mice and
588 humans. *Genome Biol.* 2010;11(6):213.

589 37. Coarfa C et al. Sexual dimorphism of the pulmonary transcriptome in neonatal
590 hyperoxic lung injury: identification of angiogenesis as a key pathway. *AJP Lung Cell*
591 *Mol Physiol.* 2017;313(6):L991-1005.

592 38. Ardini-Poleske ME et al. LungMAP: The Molecular Atlas of Lung Development
593 Program. *AJP Lung Cell Mol Physiol.* 2017;313(5):L733–L740.

594 39. Du Y et al. Lung Gene Expression Analysis (LGEA): An integrative web portal for
595 comprehensive gene expression data analysis in lung development. *Thorax.*
596 2017;72(5):481-484.

597 40. Remot A et al. Flt3 ligand improves the innate response to respiratory syncytial
598 virus and limits lung disease upon RSV re-exposure in neonate mice. *Eur J Immunol.*
599 2016; 46(4):874-884.

600 41. Chauvet S et al. EG-VEGF, BV8, and their receptor expression in human bronchi
601 and their modification in cystic fibrosis: Impact of CFTR mutation (delF508). *Am J*
602 *Physiol Lung Cell Mol Physiol.* 2015;309(3):L314–L322.

603 42. Lakhal-littleton S et al. Intracellular iron deficiency in pulmonary arterial smooth
604 muscle cells induces pulmonary arterial hypertension in mice. *Proc Natl Acad Sci*
605 *USA.* 2019;116(26):13122-13130.

606 43. Wollen EJ et al. Transcriptome profiling of the newborn mouse lung after

607 hypoxia and reoxygenation: Hyperoxic reoxygenation affects mTOR signaling
608 pathway, DNA repair, and JNK-pathway regulation. *Pediatr Res.* 2013;74(5):536–
609 544.

610 44. Dierick F et al. Resident PW1+ progenitor cells participate in vascular
611 remodeling during pulmonary arterial hypertension. *Circ. Res.* 2016;118(5):822–
612 833.

613 45. Jiang X et al. The imprinted gene PEG3 inhibits Wnt signaling and regulates
614 glioma growth. *J Biol Chem.* 2010;285(11):8472-8480.

615 46. Lingappan K, Savani RC. The Wnt signaling pathway and the development of
616 bronchopulmonary dysplasia. *Am J Respir Crit Care Med.* 2020;201(10):1174-1176.

617 47. Constantinides MG et al. A committed precursor to innate lymphoid cells. *Nature*.
618 2014;508(7496):397-401.

619 48. Oherle K et al. Insulin-like Growth Factor 1 Supports a Pulmonary Niche that
620 Promotes Type 3 Innate Lymphoid Cell Development in Newborn Lungs. *Immunity*.
621 2020;52(4):716-718.

622 49. Sadler AJ et al. BTB-ZF transcriptional regulator PLZF modifies chromatin to
623 restrain inflammatory signaling programs. *Proc Natl Acad Sci U S A.*
624 2015;112(5):1535–1540.

625 50. Zhang P et al. Hypoxia-Inducible Factor 3 Is an Oxygen-Dependent Transcription
626 Activator and Regulates a Distinct Transcriptional Response to Hypoxia. *Cell Rep.*
627 2014;6(6):1110-1121.

Figure Legends:

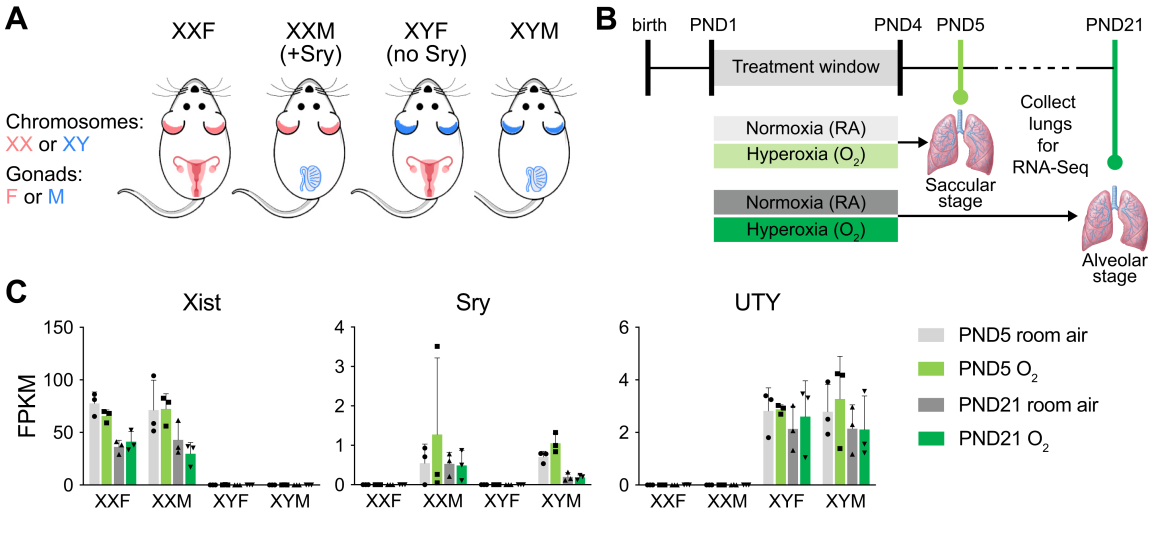

Figure 1: The FCG mouse model, neonatal hyperoxia exposure and whole lung RNA-Seq experimental model. **1A:** Mice from the FCG model; XXF (chromosomally and gonadally female), XXM (chromosomally female, gonadally male), XYF (chromosomally male, gonadally female), and XYM (chromosomally and gonadal male) were exposed to hyperoxia (95% FiO_2 from PND1-4) during the saccular stage of lung development and euthanized on PND5 and PND21. **1B:** Whole lung mRNA was subjected to RNA-Seq analysis (n=3/group). **1C:** Genotyping was confirmed by the FPKM (Fragments Per Kilobase of transcript per Million mapped reads) levels for *Uty, Sry* and *Xist*. Mean±SD.

644

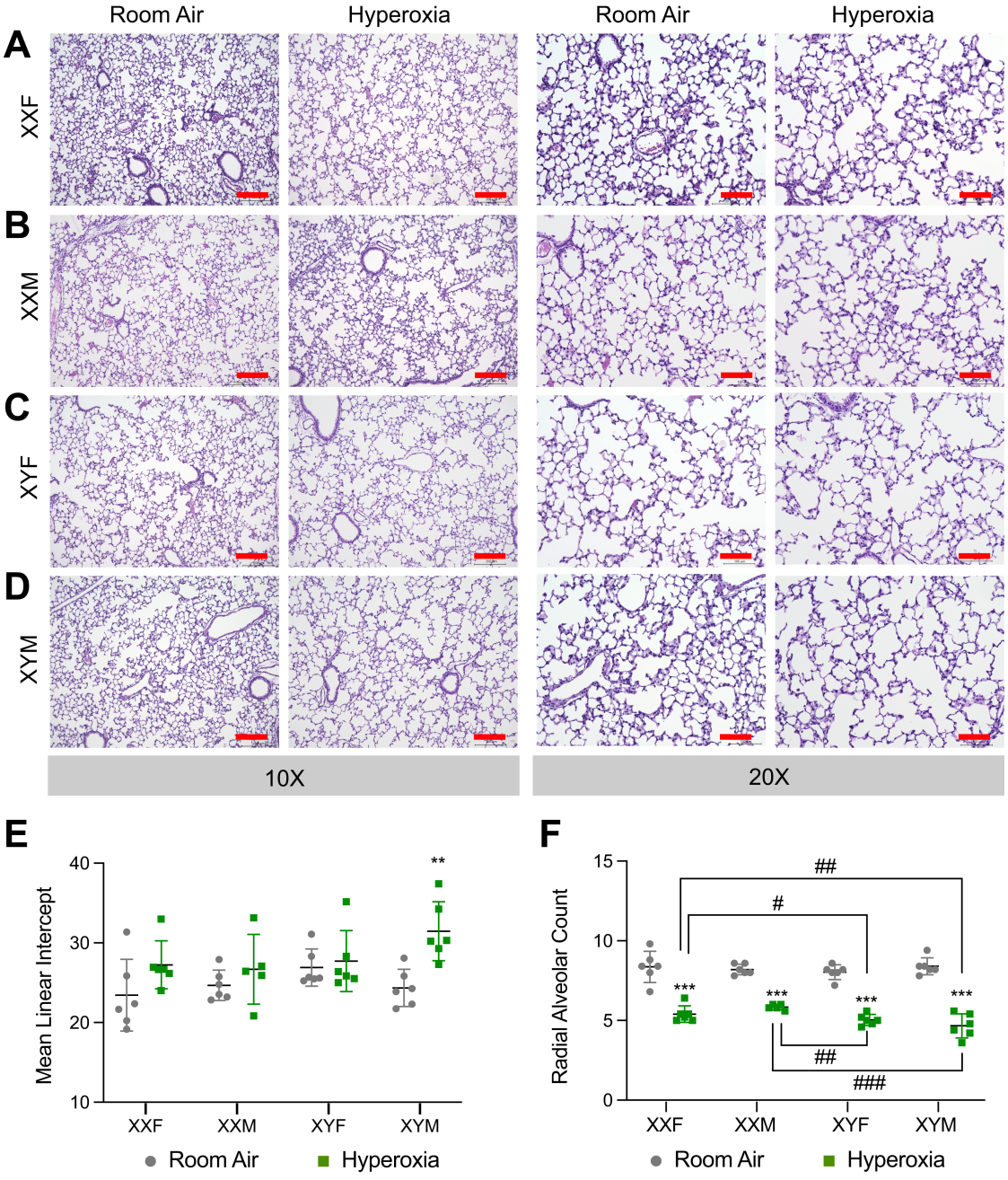

645

646 **Figure 2: Chromosomal sex but not gonadal sex had a significant impact on**

647 **alveolarization after neonatal hyperoxia exposure in mice:** Representative

648 Hematoxylin and Eosin (H&E) stained sections from male and female neonatal mice

649 exposed to room air or hyperoxia (95% FiO_2, PND 1-4) at 10x and 20x magnification

650 in XXF (**Figure 2A**), XXM (**Figure 2B**), XYF (**Figure 2C**) and XYM (**Figure 2D**) mice.
651 Lung morphometry in neonatal FCG mice (n=5-6 mice per group) exposed to
652 hyperoxia (95% FiO_2, PND 1-4) was assessed using mean linear intercept and radial
653 alveolar count. **2E**: Mean Linear Intercept (MLI) in FCG neonatal mice exposed to
654 room air or hyperoxia on PND 21. **2F:** Radial alveolar count in FCG neonatal mice
655 exposed to room air or hyperoxia on PND 21. Values are means ± SD from 5-6
656 individual animals. Statistical analysis was performed using 3-way ANOVA to assess
657 the effect of treatment, chromosomal sex and gonadal sex as well as the interactions
658 between the independent variables. Significant differences between room air and
659 hyperoxia within genotype are indicated by $^{***}P$ <0.001. Significant differences
660 between hyperoxia-exposed mice between different genotypes are indicated by $^{\#}P <$
661 0.05, $^{\#\#}P < 0.01$ and $^{\#\#\#}P < 0.001$. Scale bars equal 200 μm (10x) or 100 μm (20x).
662
663
664
665
666
667
668
669
670
671
672

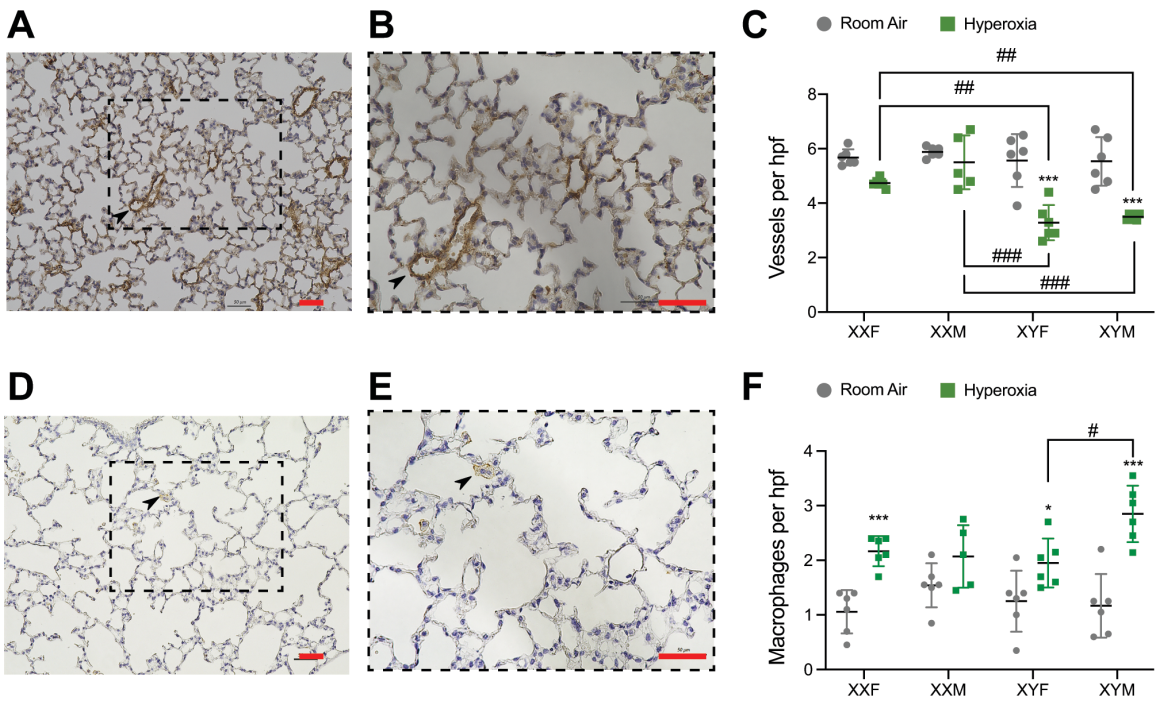

Figure 3: Arrest in angiogenesis and lung macrophages after hyperoxia exposure is differentially impacted by chromosomal and gonadal sex in neonatal mice: Immunohistochemistry and quantitation of pulmonary microvessels was done by immunostaining for endothelial-specific vWF (n=5-6 mice per group) in room air or hyperoxia (95% FiO_2, PND 1-4) in XXF, XXM, XYF and XYM mice. Representative stained sections at 20x (**3A**) and 40x magnification **(3B)**. Arrows point to brown-staining vessels. **3C:** Quantitative analyses showing number of vessels per high-power field (20x) in lungs of FCG neonatal mice. Immunohistochemistry and quantitation of macrophages was done by immunostaining for F4/80 (n=5-6 mice per group) in room air or hyperoxia (95% FiO_2, PND 1-4) in XXF, XXM, XYF and XYM mice. Representative stained sections at 20x (**3D**) and 40x magnification **(3E)**. Arrows point to brown-staining macrophages. **3F:** Quantitative analyses showing number of macrophages per high-power field (20x) in lungs of FCG neonatal mice. Values are

mean ± SD from 5-6 individual animals. Statistical analysis was performed using 3-way ANOVA to assess the effect of treatment, chromosomal sex and gonadal sex as well as the interactions between the independent variables. Significant differences between room air and hyperoxia within genotype are indicated by $^{***}P < 0.001$. Significant differences between hyperoxia-exposed mice between different genotypes are indicated by $^{\#\#}P < 0.01$ and $^{\#\#\#}P < 0.001$. Scale bars equal 50 μm.

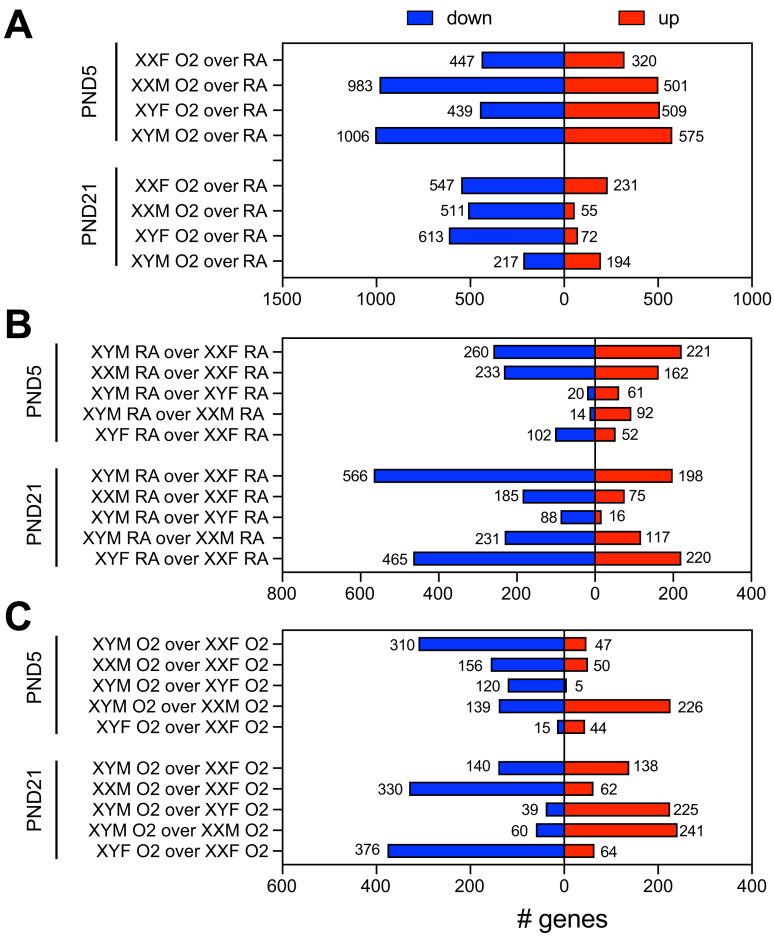

Figure 4: Transcriptomic analysis of FCG mice shows a robust and genotype specific response to neonatal hyperoxia exposure: The total number of up- and down-regulated differentially expressed genes (DEGs) are shown in Figure 4. The hyperoxia response in each genotype is shown in **Figure 4A**, while differences between the genotypes in normoxia and under hyperoxic conditions are shown in **Figure 4B and Figure 4C** respectively.

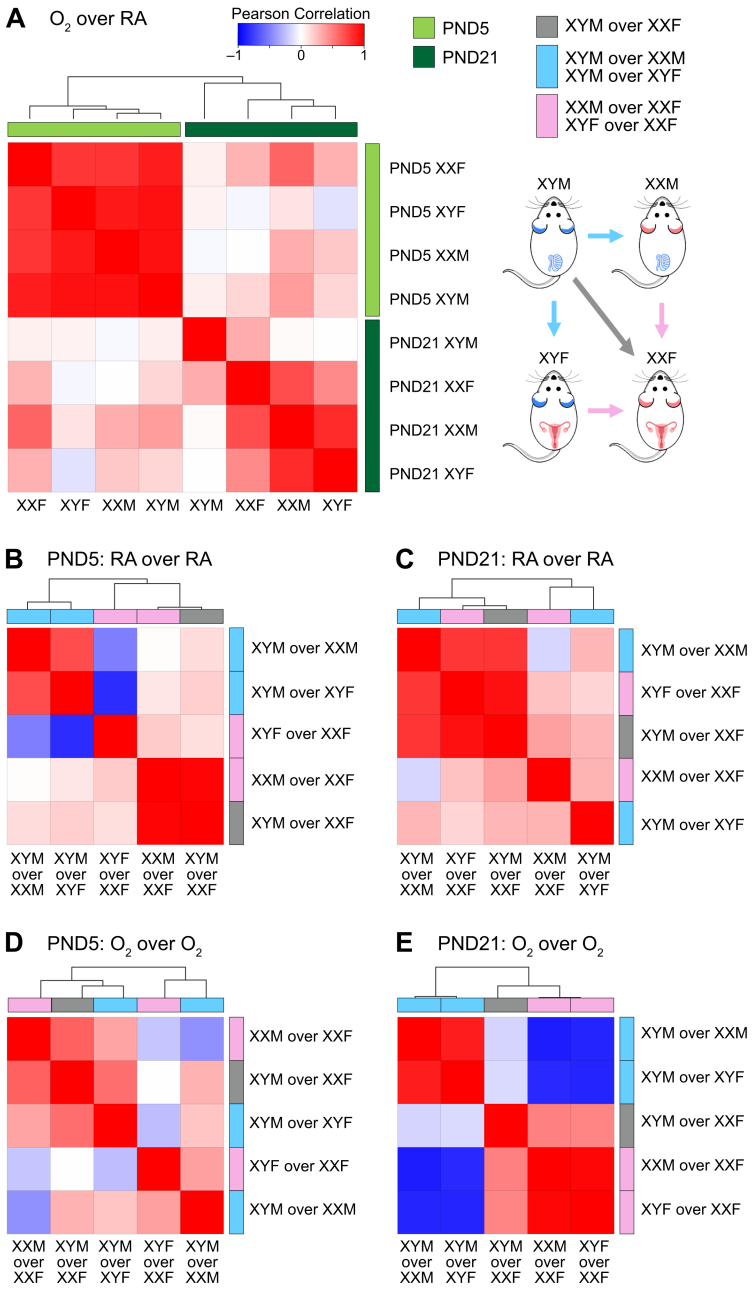

Figure 5: Gene expression signatures in the FCG murine neonatal lungs show striking correlation patterns superimposed on the human lung transcriptome. To compare signatures (differentially expressed genes; DEGs) in our pulmonary murine models, we used transcriptome profiles of 578 healthy human adult lung samples compiled by the GTEx consortium to assess genotype/transcriptome relationships in phenotypically

healthy individuals. We computed summed z-scores for each human individual and each FCG signature and assessed inter-signature correlations. There is a clear separation between the PND5 and the PND21 hyperoxia signatures (**Figure 5A**). The acute response signatures at PND5 show very strong correlation across all genotypes. At PND21, the hyperoxia responses in gonadal or chromosomal females XXF, XXM, and XYF cluster together, apart from the response in the chromosomal and gonadal male XYM genotype. Correlation between genotype summed z-scores are shown in room air at PND5 (**Figure 5B**) and PND21 (**Figure 5C**) and hyperoxia at PND5 (**Figure 5D**) and PND21 (**Figure 5E**).

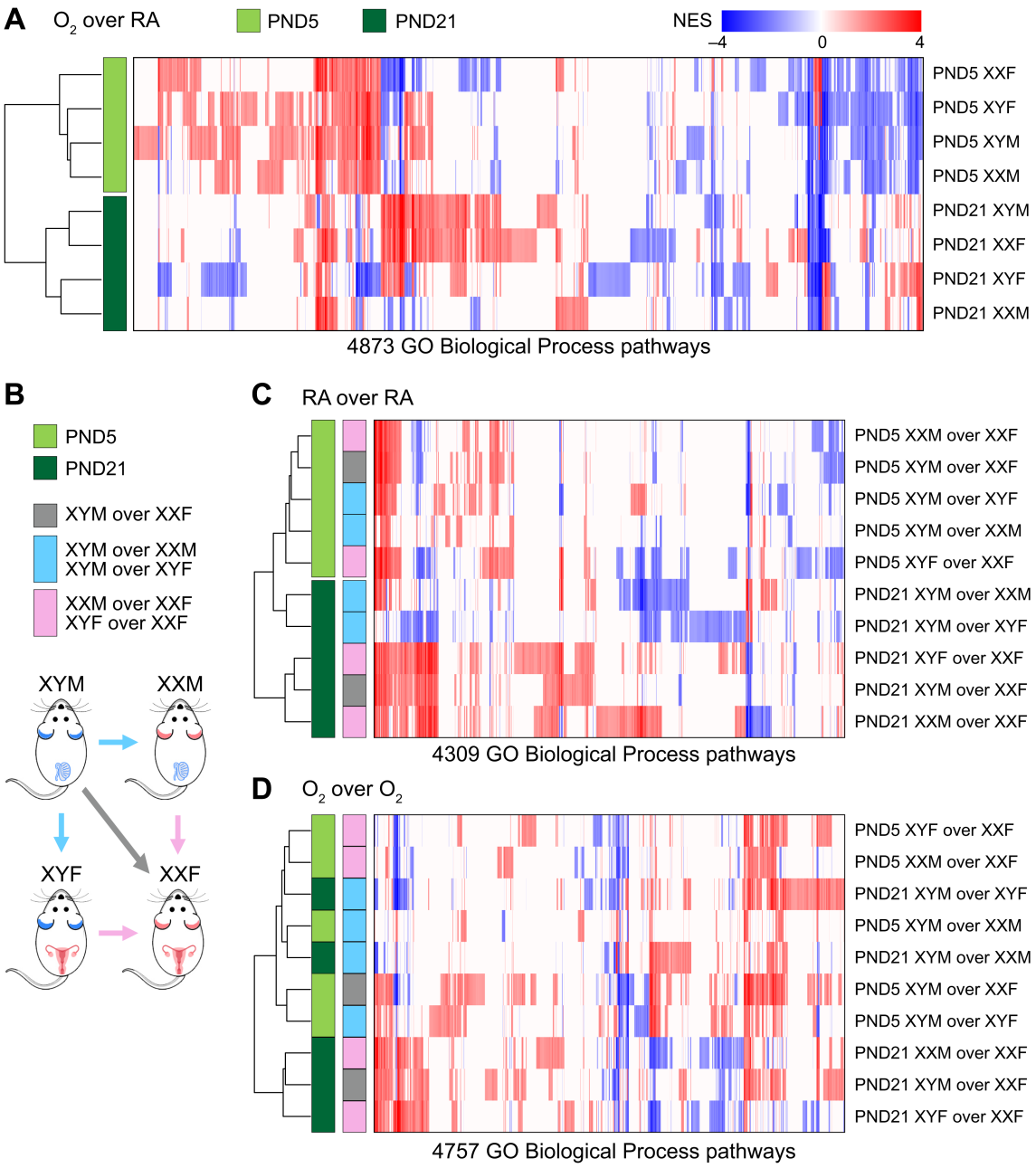

747

748 **Figure 6: Pathway-based cluster analysis for transcriptomic footprints of**

749 **hyperoxia exposure or of genotype differences in the FCG mouse model:** Gene

750 Set Enrichment Analysis (GSEA) was used to quantify enrichment of GO Biological

751 Process pathways. Hierarchical clustering and heatmaps were generated for the

752 transcriptomic footprints using the significant normalized enrichment scores (NES).

Pathway-based clustering of response to hyperoxia across all genotypes show striking and distinct clustering between the PND5 and PND21 responses (**Figure 6A**). Pathway-based clustering of inter-genotype differences under room air conditions also show robust clustering with the time points (**Figure 6B**). Hierarchical clustering of enriched biological pathways under hyperoxia of inter-genotypes comparisons does not show clustering with respect to post-natal day (**Figure 6C**).

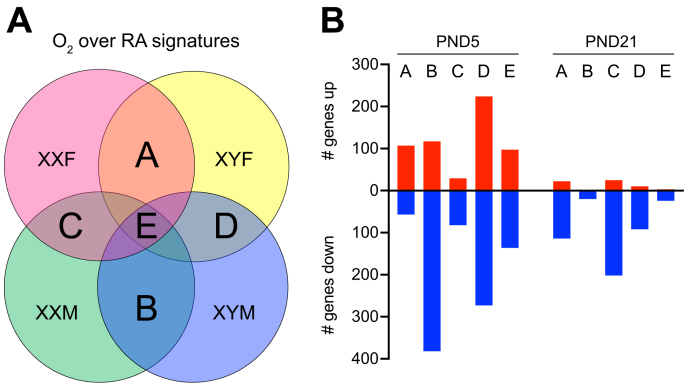

A: Female gonad overlap (XXF, XYF)
B: Male gonad overlap (XXM, XYM)
C: XX chromosome overlap (XXF, XXM)
D: XY chromosome overlap (XYF, XYM)
E: common hyperoxia response

Figure 7: Distribution and Overlap of gene signatures in the FCG mouse model based on the gonadal and chromosomal sex: The 4-way venn diagram (**Figure 7**) shows the schematic used to discern the number of genes (up- and down-regulated) based on female gonadal response (area A; common genes between XXF and XYF), male gonadal response (area B; common genes between XXM and XYM), female chromosomal response (area C; common genes between XXF and XXM), and male chromosomal response (area D; common genes between XYF and XYM). Area E (which represents the common differentially expressed genes (DEGs) across all the genotypes) was not included for the groups above. The adjoining graph provides the number of genes from each of these groups.

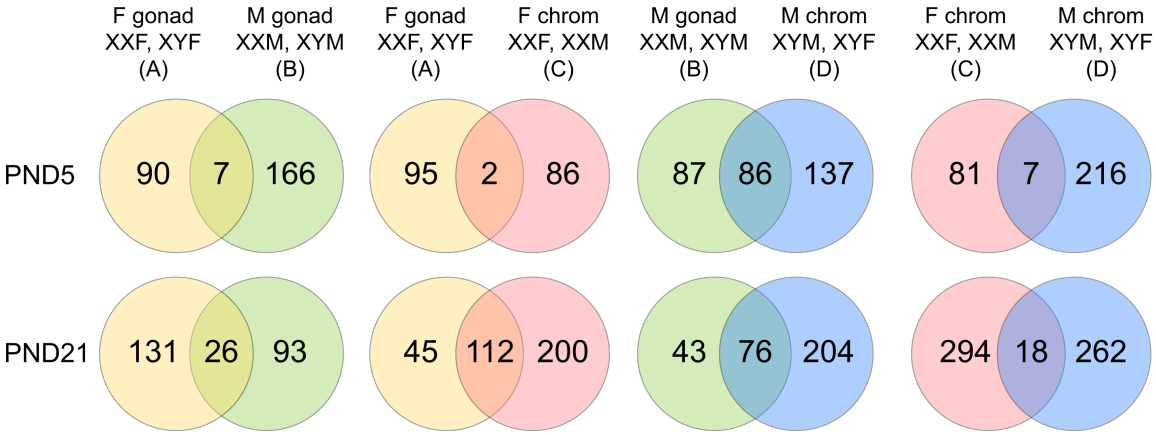

Figure 8: Distribution and Overlap of biological pathways based on the gonadal and chromosomal sex in the FCG mouse model: Analysis of enriched pathway from the Gene Ontology Biological Processes compendium in DEGs and the overlap based on the gonadal or chromosomal sex at PND5 and PND21. The number of biological pathways are specified within the Venn diagrams.

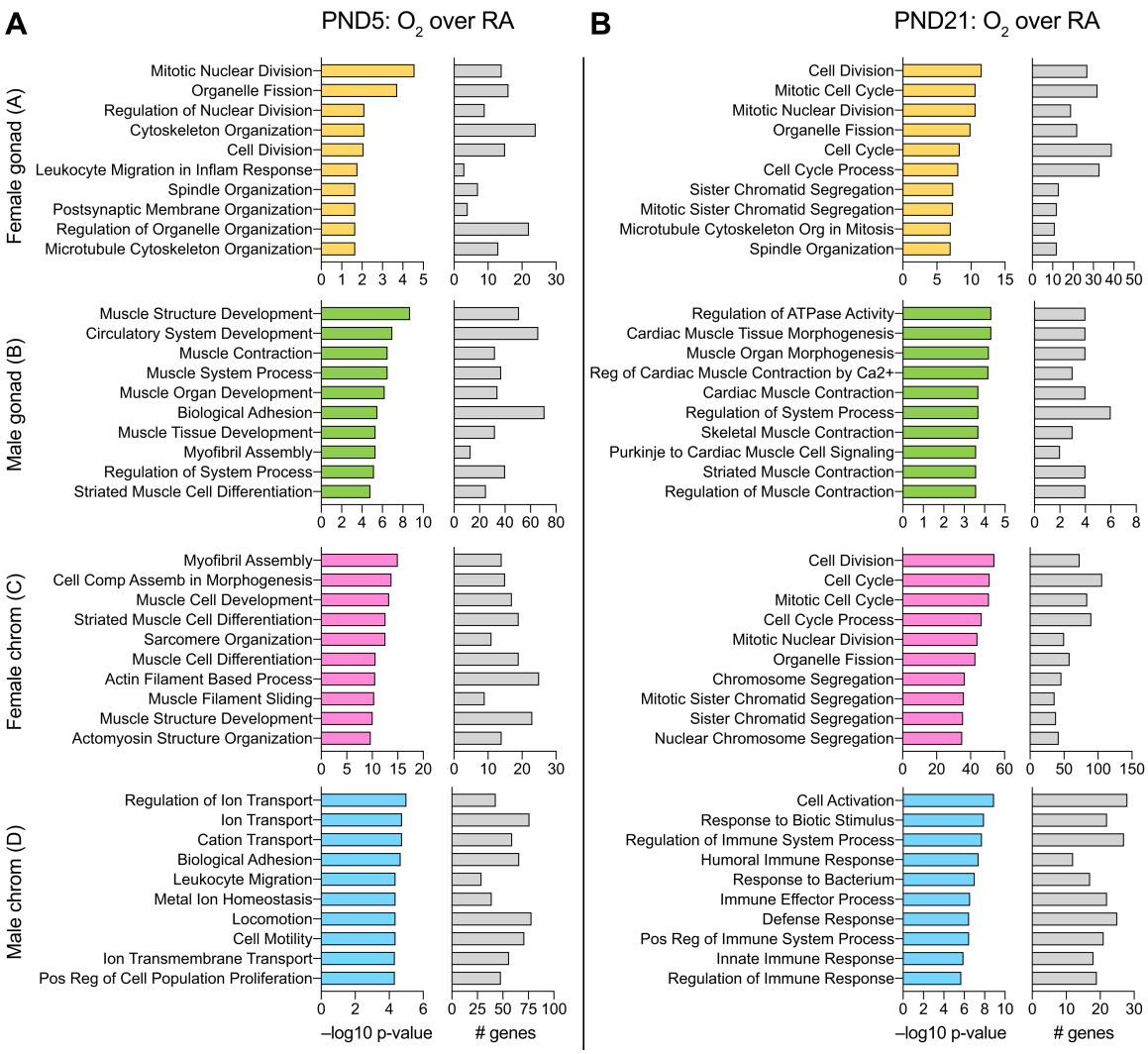

Figure 9: Enriched biological pathways are distinct based on the gonadal or chromosomal sex in the FCG mouse model at PND5 and PND21 after hyperoxia exposure: The top ten Gene Ontology Biological Processes pathways enriched in mice with female gonads (A; XXF and XYF), male gonads (B; XXM and XYM), female chromosomes (C; XXF and XXM), and male chromosomes (D; XYM and XYF) are shown. The significance of enriched pathways as -log10(p-value) and the number of included DEGs in the pathways are depicted.

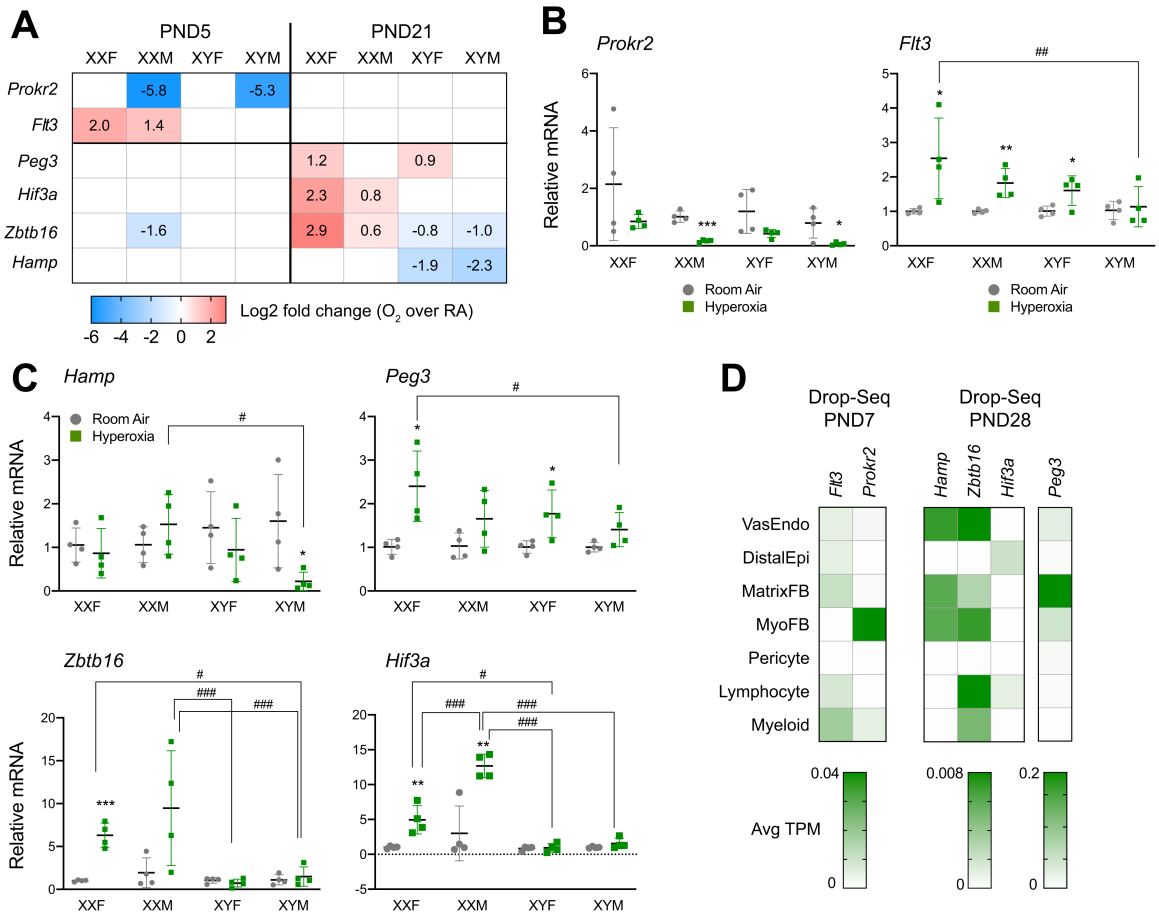

Figure 10: Independent validation of RNA-Seq results for selected genes with qRT-PCR and cell-specific expression in neonatal mice: A subset of highly expressed differentially expressed genes were validated in an independent cohort of FCG neonatal mice. The fold change of the selected genes in the RNA-Seq experiment are shown in **Figure 10A** and the changes in the qRT-PCR experiments are shown in **Figure 10B** for DEGs at PND5 (*Flt3* and *Prokr2*) and **Figure 10C** for DEGs at PND21 (*Hamp, Peg3, Zbtb16 and Hif-3α*). Values are mean ± SD from 4 individual animals. Analysis done by 3-way ANOVA to assess the effect of treatment, chromosomal sex and gonadal sex as well as the interactions between the independent variables. Significant differences between room air and hyperoxia within genotype are

indicated by *P<0.05, **P<0.01, and ***P <0.001. Significant differences between hyperoxia-exposed mice between different genotypes are indicated by $^{\#}P < 0.05$, $^{\#\#}P < 0.01$, and $^{\#\#\#}P < 0.001$. For these selected genes, we also evaluated the expression in publicly available neonatal lung single-cell expression database (LungMAP) in **Figure 10D.**

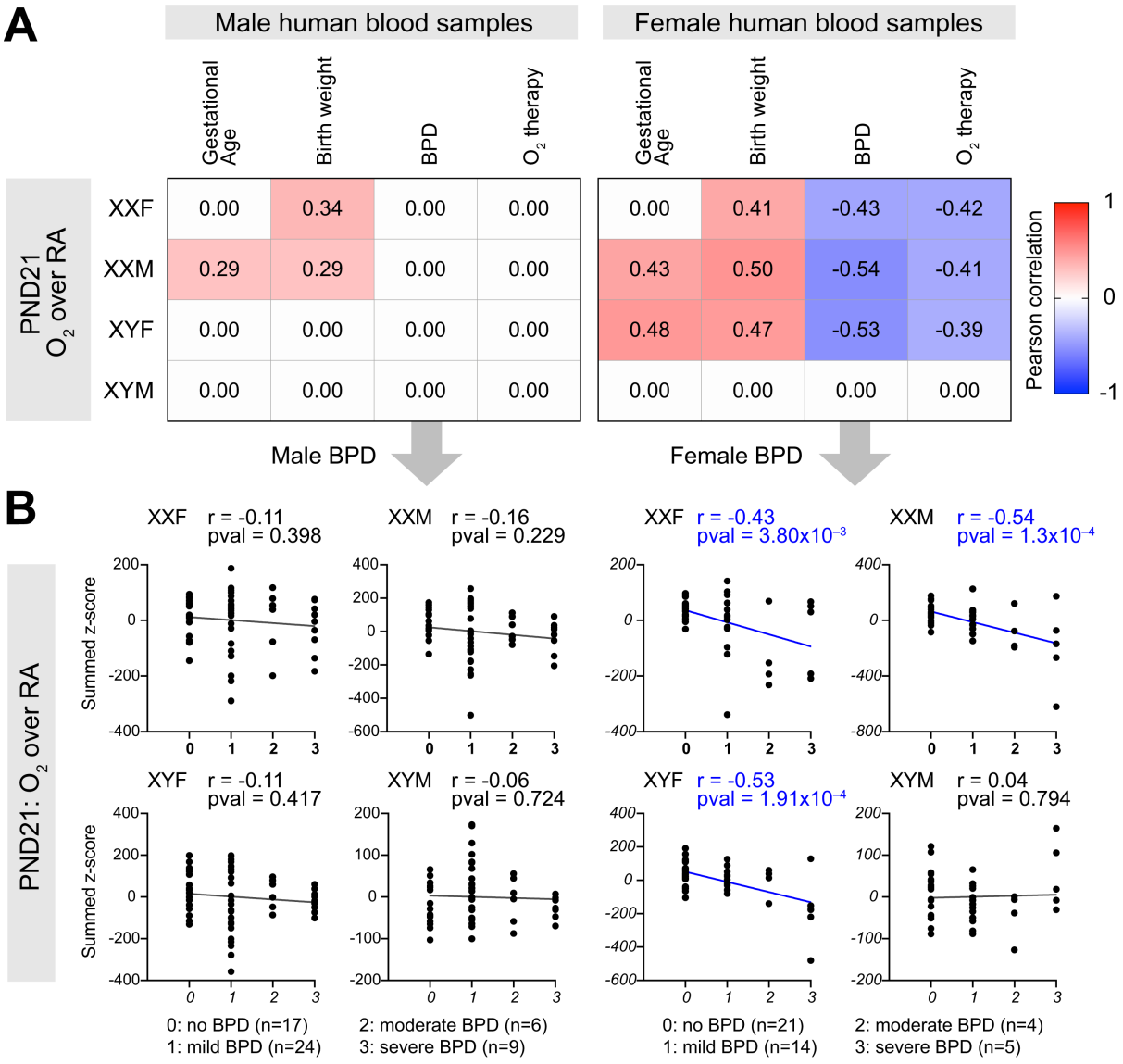
A
Male human blood samples
Female human blood samples
Gestational Age
Birth weight
BPD
O2 therapy
PND21 O2 over RA
XXF 0.00 0.34 0.00 0.00 | 0.00 0.41 -0.43 -0.42
XXM 0.29 0.29 0.00 0.00 | 0.43 0.50 -0.54 -0.41
XYF 0.00 0.00 0.00 0.00 | 0.48 0.47 -0.53 -0.39
XYM 0.00 0.00 0.00 0.00 | 0.00 0.00 0.00 0.00
Pearson correlation
1
0
-1
Male BPD
Female BPD
B
PND21: O2 over RA
XXF r = -0.11 pval = 0.398
XXM r = -0.16 pval = 0.229
XXF r = -0.43 pval = 3.80x10-3
XXM r = -0.54 pval = 1.3x10-4
XYF r = -0.11 pval = 0.417
XYM r = -0.06 pval = 0.724
XYF r = -0.53 pval = 1.91x10-4
XYM r = 0.04 pval = 0.794
Summed z-score
0: no BPD (n=17)
1: mild BPD (n=24)
2: moderate BPD (n=6)
3: severe BPD (n=9)
0: no BPD (n=21)
1: mild BPD (n=14)
2: moderate BPD (n=4)
3: severe BPD (n=5)
C
PND21: O2 over RA
Human blood
XXF XXM XYF XYM BPD O2
GO Pathway:
Normalized Enrichment Score
-7 0 7
-4.01 -1.64 -2.46 3.73 5.97 6.11 Keratinization
-3.71 -1.79 -2.43 3.35 3.89 4.03 Cornification
-3.04 -4.51 -4.41 1.72 2.11 2.07 Sarcomere Organization
-2.70 -4.02 -3.49 1.69 2.48 2.37 Cellular Component Assembly in Morphogenesis
-2.59 -4.44 -2.83 3.52 4.16 4.40 Muscle Contraction
-2.53 0.00 0.00 0.00 3.16 3.46 Vascular Endothelial Growth Factor Receptor Signaling Pathway
-2.26 -2.15 0.00 0.00 1.61 1.54 Mitotic Cell Cycle Checkpoint
-2.25 0.00 -1.80 0.00 2.00 2.03 T Helper 1 Cell Cytokine Production
-2.18 -2.20 0.00 0.00 1.71 1.75 Positive Regulation of Cell Cycle
-2.14 0.00 -1.83 0.00 1.61 1.43 Sphingolipid Metabolic Process
-2.06 -2.74 -1.63 0.00 3.89 3.59 Reproduction
-2.01 0.00 0.00 0.00 1.92 1.80 Regulation of DNA Binding Transcription Factor Activity

Figure 11. Murine hyperoxia signatures associate with blood transcriptomes in human newborns at risk of BPD. Blood transcriptome at PND28 from a cohort of human newborns evaluated for development of BPD was obtained. **A.** The distribution of summed z-scores for hyperoxia gene signatures from all our murine models, at PND21, was evaluated against four clinical variables: gestational age, birth weight, BPD status and need for oxygen at 28 days of post-natal age. Pearson correlation coefficient is shown for significant correlation ($p<0.05$) **B.** Distribution of summed z-scores for hyperoxia signatures in murine models at PND21 are shown in the human newborn blood samples collected at PND28, stratified by biological sex and by BPD status (no BPD, mild, moderate and severe). Association was evaluated using the parametric Pearson correlation, with the Pearson correlation coefficient (r) and p-values indicated. **C.** Selected Gene Ontology pathways and their normalized enrichment scores induced in the blood transcriptome of BPD patients at PND28, while suppressed after hyperoxia exposure in lungs of feminized mice and either induced or not differentially modulated in XYM mice at PND21 are shown in the heat map (**Figure 11C**).

856 Table 1: Validation by qRT-PCR

Validated genes	RNA-Seq	qRT-PCR validation	3-way ANOVA significance[A]	Biological relevance
PND5				
Flt3 (FMS-like tyrosine kinase 3)	↑ XXF, XXM	↑ XXF, XXM	Tt, CS and CSxTt	Protection against RSV-mediated airway disease by increasing the lung dendritic cell population (40).
Prokr2 (prokineticin receptor 2)	↓ XXM,XYM	↓ XXM,XYM	Tt, GS	Peribronchial vascular remodeling in cystic fibrosis (41).
PND21				
Hamp (Hepcidin antimicrobial peptide)	↓ XYM, XYF	↓ XYM	CSxTt	Maintains intracellular iron stores (42), decreases pulmonary arterial hypertension (PAH)
Peg3 (Paternally expressed 3)	↑ XXF, XYF	↑ XXF, XYF	Tt	Increased in PAH, hyperoxia, inhibits Wnt signaling. (43) (44) (45) (46).
Zbtb16 (zinc finger and BTB domain containing 16)	↑ XXF, XXM ↓ XYM, XYF	↑ XXF	Tt, CS,GS, CSxTt, GSxTt	Marker of committed innate lymphoid cell progenitors, which give rise to type 3 innate lymphoid cells (ILC3s)(47). ILC3s are decreased in BPD (48). Chromatin modifying effects and decreases inflammation (49).
Hif-3α (Hypoxia inducible factor-3 alpha)	↑ XXF, XXM	↑ XXF, XXM	Tt, CS, GS, CSxTt, GSxTt, CSxGSxTt	Oxygen-dependent transcription factor with hypoxia-dependent and independent effects. Some downstream genes overlap with Hif-1α (50).

[A] Tt: treatment; CS: chromosomal sex; GS: gonadal sex
"x" represents interaction between the independent variables

857